

## Nano-optical Properties of Sputtered Indium Tin Oxide on Black Silicon for Heterojunction Solar Cells

Auwal Abdulkadir<sup>1\*</sup>, Azlan Abdul Aziz<sup>2</sup> and Mohd Zamir Pakhuruddin<sup>2,3\*</sup>

<sup>1</sup>*Department of Physics, Umaru Musa Yar'adua University, P. M. B. 2218 Katsina, Nigeria*

<sup>2</sup>*Photovoltaic Materials and Devices, School of Physics, Universiti Sains Malaysia, 11800 Minden, Penang, Malaysia*

<sup>3</sup>*Institute of Nano Optoelectronics Research and Technology (INOR), Universiti Sains Malaysia, 11800 USM, Penang, Malaysia*

*Corresponding authors: zamir@usm.my, auwal.abdulkadir@umyu.edu.ng*

Accepted: 9 December 2022; Published: 21 January 2023

### ABSTRACT

This study investigates surface morphological and optical properties of sputtered indium tin oxide (ITO) thin films on black silicon (b-Si) fabricated by metal-assisted chemical etching (MACE) for potential application in heterojunction solar cells. After depositing 50 nm, 80 nm, and 140 nm of ITO, electron dispersive X-ray (EDX) confirms the presence of In, O, and Sn elements in weight percentage (wt.%) on b-Si nanowires. With ITO on b-Si, weighted average reflection (WAR) decreases compared to ITO on reference c-Si within the wavelength region of 300-1100 nm. This is due to the refractive index grading effect, which improves light-coupling into the b-Si absorber. In the solar cells measured under white LED illumination (at 47 mW/cm<sup>2</sup>) at room temperature (25°C), the ITO/c-Si/NiO solar cell (reference) demonstrates short-circuit current density ( $J_{sc}$ ) of 3.10  $\mu\text{A}/\text{cm}^2$ . In comparison, the ITO/b-Si/NiO solar cell achieves an enhanced  $J_{sc}$  of 3.96  $\mu\text{A}/\text{cm}^2$  at a slightly higher open-circuit voltage ( $V_{oc}$ ). This represents 28% of  $J_{sc}$  enhancement when compared to the reference cell. The enhancement in the  $J_{sc}$  of the b-Si solar cell owes to the increased light absorption in the b-Si absorber within the 300-1100 nm wavelength region.

**Keywords:** *Indium tin oxide, black silicon, nanowires, heterojunction*

## INTRODUCTION

Indium tin oxide (ITO) is a promising ARC material and front electrode on crystalline silicon (c-Si) solar cells to increase light absorption and enhance photocurrent [1, 2]. This is due to its high conductivity, stable chemical properties, wide band gap (3.3-4.3 eV) and high optical transmission exceeding 80% in the visible wavelength region. ITO's applications on p-type c-Si as an emitter to demonstrate heterojunction solar cells have also been reported [1-3]. This owes to the ITO's native n-type conductivity and Schottky barrier formation when contacted with p-type c-Si [3-5]. Chemical vapour deposition (CVD), ultrasonic spray, magnetron sputtering, pulsed laser deposition (PLD), and sol-gel are the most common deposition methods to prepare ITO for the said applications [3-8]. In ITO/p-type c-Si heterojunction architecture, incident photons in the short wavelength region will be harvested within the front ITO layer. In contrast, photons in the visible and near-infrared regions will be harvested by the p-type c-Si. Eliminating heavily-doped emitter associated with high-temperature diffused emitter in c-Si/b-Si solar cells is another merit of ITO/p-type c-Si heterojunction solar cells [8, 9].

Nanotexturing of the c-Si wafer surface to produce nanotextures (e.g. porous structures, nano spikes, nano-cones, nanowires or nano-hillocks) with dimensions smaller than the wavelength of the incident light (called "black silicon" (b-Si)) is a promising approach to reduce broadband light reflection from the c-Si [10-12]. The nanotexturing is usually fabricated by reactive ion etching (RIE), laser irradiation, plasma immersion ion implantation (PIII) or electroless metal-assisted wet chemical etching (MACE). Marikkannu et al. [13] reported a jet nebuliser spray (JNS) pyrolysis method for depositing ITO on porous c-Si for application as heterojunction solar cells. In their study, the enhanced optical absorption provided by the porous c-Si was relatively low. Besides, Schulz et al. reported a 1 cm<sup>2</sup> semiconductor-insulator-semiconductor (SIS: ITO/SiO<sub>2</sub>/b-Si/Al) solar cell with enhanced optical absorption by sputtering 500 nm of ITO on nanotextured b-Si fabricated via RIE process [14]. Owing to light trapping by nanotextures, the b-Si solar cell tested under standard test condition (STC) exhibits short-circuit current density ( $J_{sc}$ ) of 24.05 mA/cm<sup>2</sup> compared to 20.22 mA/cm<sup>2</sup> for the reference cell (ITO/SiO<sub>2</sub>/c-Si/Al). However, the b-Si solar cell exhibits low open-circuit voltage ( $V_{oc}$ ) (420 mV) when compared to the reference cell (460 mV). The lower  $V_{oc}$  is attributed to incomplete ITO coverage on the b-Si nanotextures and increased surface recombination by high aspect ratio nanotextures fabricated by the RIE. To improve the quality of the ITO on the b-Si, there is a need to replace the high aspect ratio b-Si by the RIE process with a low aspect ratio b-Si fabricated by the MACE process.

In this work, b-Si is fabricated by a two-step MACE process. Direct current (DC) magnetron sputtering technique is utilised to deposit ITO with different thicknesses (50 nm, 80 nm, and 140 nm) on the b-Si nanowires and flat c-Si (as a reference). Then, the ITO's surface morphological and optical properties on b-Si and c-Si references are characterised. To verify the enhancement in light absorption and photocurrent for the ITO on b-Si relative to ITO on flat c-Si, solar cells utilising p-type b-Si absorbers are fabricated from the optimised ITO film thickness. The electrical

properties of the cells are characterised under a white light illumination system (LED-based solar simulator). Then, the findings from the electrical characterisation are analysed and discussed.

## EXPERIMENTAL

P-type 250  $\mu\text{m}$ -thick monocrystalline silicon (mono c-Si) wafers with 1–10  $\Omega\cdot\text{cm}$  resistivity are used as the starting substrates. B-Si nanowires on the p-type c-Si wafers surfaces are obtained by the MACE method, which involves silver nitrate ( $\text{AgNO}_3$ ; 2.5 wt.% in  $\text{H}_2\text{O}$ ) and hydrofluoric acid (HF) with 20 g/mol (49%). The process involves dipping the c-Si wafers in a 5:6 (110 ml) molar ratio solution prepared in a polypropylene beaker at room temperature for 30 s to deposit Ag nanoparticles (Ag NPs). This is followed by etching the wafers in 2:1:5 HF: $\text{H}_2\text{O}_2$ :DI  $\text{H}_2\text{O}$  (80 ml) solution for 20 s, which produces the b-Si nanowires. After this process, the residual Ag NPs on the wafers are removed using concentrated  $\text{HNO}_3$  (60%) in a sonication bath. The b-Si wafers are then dipped in HF solution for 15 s and dried with  $\text{N}_2$  [15].

ITO layer with thicknesses of 50 nm, 80 nm and 140 nm is then sputtered on the p-type c-Si reference and the wafers with b-Si nanowires by DC magnetron sputtering, using ITO target with a purity of 99.99%. Besides, the ITO films are also sputtered on a glass substrate for optical characterisation. For the deposition, a base pressure of  $5 \times 10^{-5}$  mbar, DC power of 100 W, a deposition rate of 1.2  $\text{\AA}/\text{s}$ , and an argon flow rate of 15 sccm are used. This work adopts dopant-free asymmetric heterocontacts (DASH) device architecture for solar cell fabrication. This architecture uses ITO and NiO to extract electrons and holes, respectively. Front silver (Ag) contacts are thermally evaporated on top of the ITO films using a shadow mask for the Hall effect and solar cell samples. The samples are then annealed at 200°C in  $\text{N}_2$  ambient for 30 min to produce an excellent ohmic contact between Ag and ITO. 15 nm of NiO layer is then sputtered on the rear side of the b-Si and reference c-Si using radio frequency (RF) sputtering. RF power of 150 Watt is used. This is followed by the deposition of 200 nm thick aluminium (Al) back contact using DC sputtering (with a power of 150 W).

Surface morphological properties of ITO on c-Si and b-Si are characterised using Field Emission Scanning Electron Microscopy (FESEM). Besides, energy-dispersive X-ray spectroscopy (EDX) is used to study the elemental mapping of ITO thin films on b-Si nanowires. Transmission and reflection of ITO on glass, flat reference p-type c-Si and b-Si are measured by Cary 5000 UVVISNIR spectrophotometer over 300–1100 nm wavelength region. The spectrophotometer is equipped with an integrating sphere. The optical absorption coefficient ( $\alpha$ ) for ITO films on glass is calculated using equation (1) at different wavelengths using the reflection and transmission data from the optical characterisation results.

$$\alpha = \frac{1}{t} \ln \left[ \frac{(1-R)^2}{T} \right] \quad (1)$$

In equation (1),  $t$  is ITO film thickness,  $R$  is total reflection, and  $T$  is transmission [16]. The optical band gap ( $E_g$ ) of ITO thin films on glass is then obtained using Tauc's relation as presented in equation (2) by plotting  $(\alpha h\nu)^{1/n}$  against  $h\nu$  and extrapolating its straight-line to where  $h\nu=0$ . In this equation,  $A$  is constant,  $h\nu$  is photon energy, and  $n=0.5$  represents direct electron transition in ITO [16].

$$\alpha h\nu = A(h\nu - E_g)^n \quad (2)$$

The weighted average reflection (WAR%) of ITO on glass, reference p-type c-Si and b-Si is calculated using Equation 3 [19]. This is done by integrating the reflection result with AM1.5G solar spectrum over 300-1100 nm wavelength region. In Equation 3,  $R(\lambda)$  denotes the reflection while  $S(\lambda)$  is the AM1.5G solar spectrum.

$$WAR = \frac{\int_{300 \text{ nm}}^{1100 \text{ nm}} R(\lambda)S(\lambda)d\lambda}{\int_{300 \text{ nm}}^{1100 \text{ nm}} S(\lambda)d\lambda} \quad (3)$$

Absorption ( $A$ ) in ITO on glass, c-Si reference b-Si is calculated using  $A=(100-R-T) \%$ . Transmission ( $T$ ) is assumed to be zero for cases involving p-type c-Si and b-Si since the bulk p-type c-Si wafer is opaque. Hence  $A$  is approximately  $(100-R)\%$  [17,18]. Hall effect system is used to determine the electrical properties ((carrier concentration ( $n_e$ ), sheet resistance ( $R_s$ ) and charge carrier mobility ( $\mu_e$ )) of the ITO film on the b-Si samples. Current-voltage behaviour of the ITO/b-Si/NiO<sub>x</sub> and ITO/c-Si/NiO<sub>x</sub> reference solar cells are measured with white light illumination of 47 mW/cm<sup>2</sup> using an LED-based solar simulator at room temperature. Even though the measurement uses an LED system, relative PV performance between the solar cells can still be investigated.

## RESULTS AND DISCUSSION

Figure 1 presents the optical properties of ITO films (50 nm, 80 nm and 140 nm) sputtered on the glass substrate. Note that the ITO film faces the incident light during the measurement for this characterisation. This is carried out to assess the optical band gaps of the ITO films and to understand their properties prior to being deposited on c-Si and b-Si.

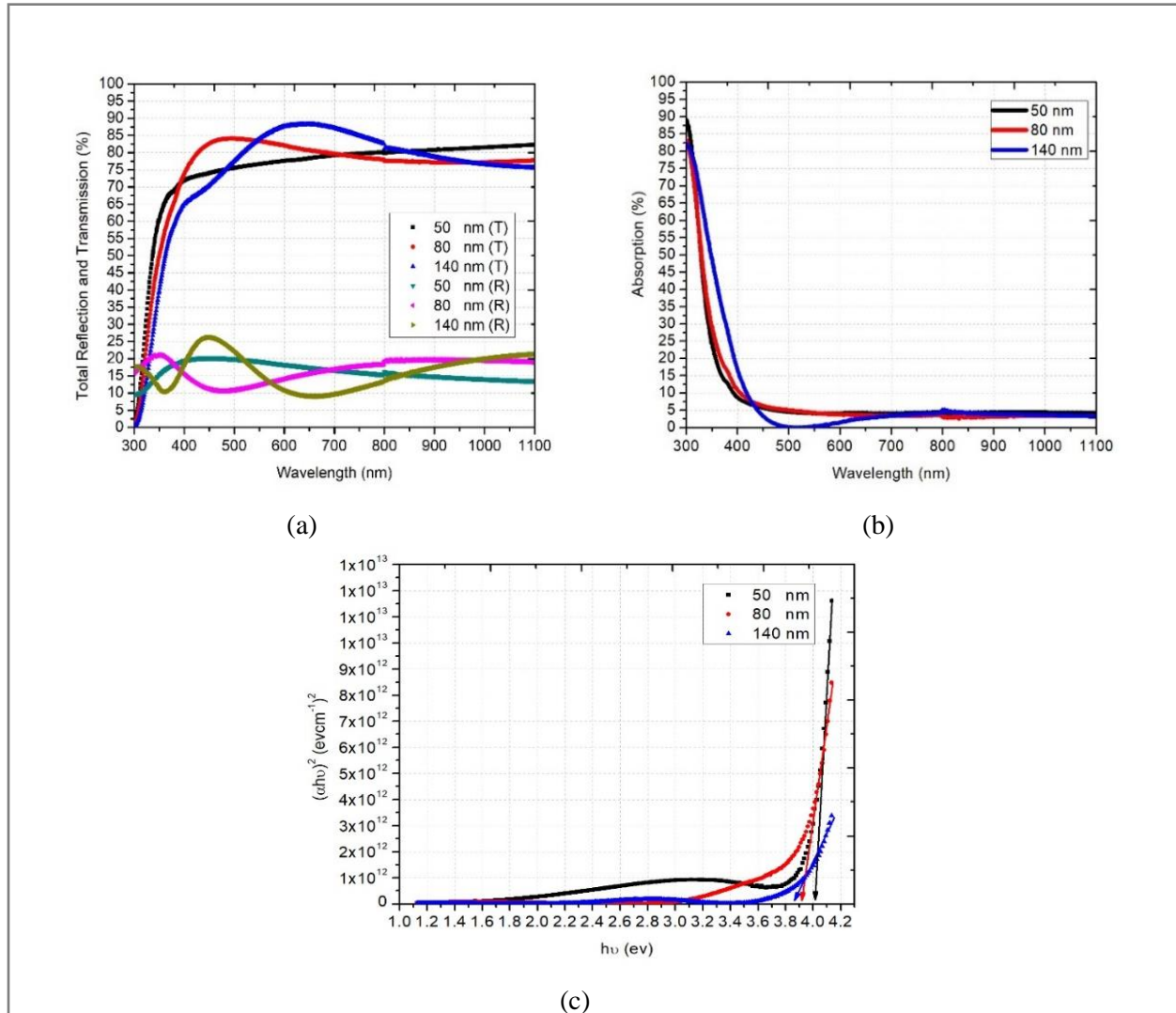


**Figure 1:** (a) Total reflection and transmission (b) Parasitic absorption calculated using;  $A=(100-R-T)$  % (c) Tauc's plot for ITO thin films on glass

From Figure 1 (a), an average transmission of 75.2%, 74.9%, 75.5% and WAR of 16.3%, 16.9%, and 16.3% are obtained for 50 nm, 80 nm, and 140 nm ITO films, respectively, within the 300-1100 nm wavelength region. Besides, 8.5%, 8.2% and 9.2% average parasitic absorption are demonstrated in the ITO films, as shown in Figure 1 (b). The parasitic absorption is calculated based on  $A=(100-R-T)$  %. Besides, a shift in optical absorption edges (which can also be viewed as minimum reflection and maximum transmission peaks) to higher wavelengths is observed with

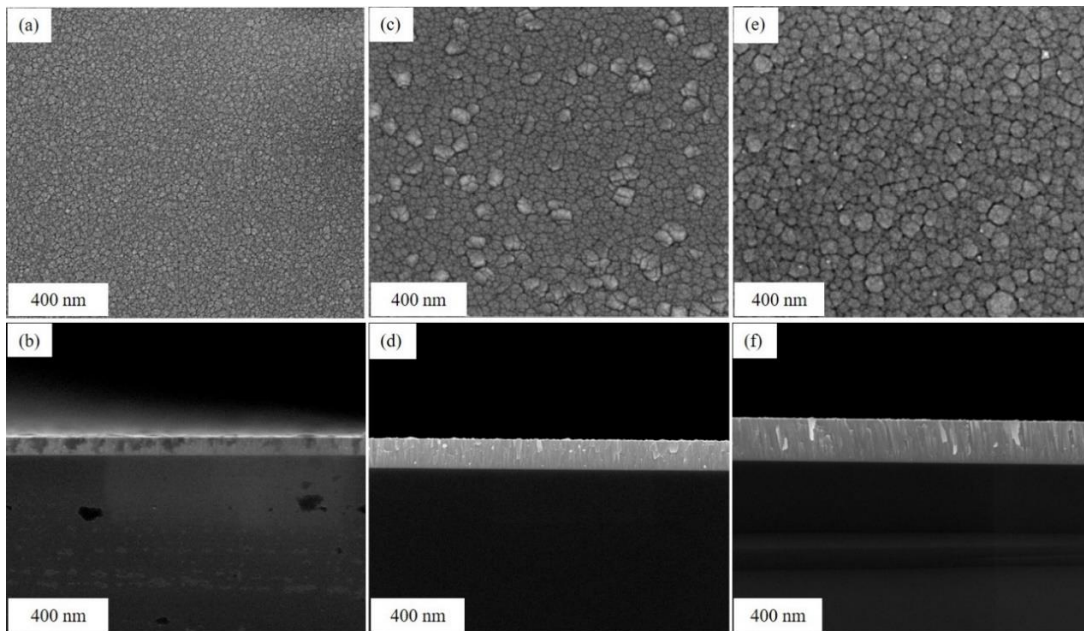
increasing ITO thickness, following the Burstein-Moss shift effect [19, 20]. Apart from this, 50 nm of ITO shows low surface reflection and high optical transmission at the 300-400 nm wavelength region. This signifies low parasitic optical absorption for this thickness within the 300-400 nm wavelength region, compared to 80 nm and 140 nm of ITO films. The steepest optical transmission at around 450 nm for 80 nm ITO film and 600 nm for 140 nm film is potentially due to lower defect density within these films [5, 19, 20].

For 50 nm of ITO, an optical band gap of 4.0 eV is obtained (Figure 1 (c)). When the film thickness is increased to 80 nm and 140 nm, the band gap reduces to 3.90 eV and 3.85 eV, respectively. The decrease in the band gap with increasing thickness confirms lower defect density near the band edges for these films than lower ITO thickness (50 nm). This has also been reported by other findings [19, 20]. For 80 nm of ITO, the optical absorption edge moves slightly to around 450 nm wavelength region, which is why it has a slightly lower band gap of 3.90 eV compared with 50 nm film thickness [19, 20]. ITO with 140 nm thickness on glass exhibits the lowest band gap of 3.85 eV. Furthermore, this film exhibits the highest optical transmission at 600-800 nm wavelength region with low reflection and parasitic absorption compared to 50 nm and 80 nm films in the same wavelength region. This suggests the optimum thickness to fabricate ITO/c-Si and ITO/b-Si interfaces since the 600-800 nm region is close to the AM1.5G solar spectrum's peak and represents the optical power of the LED spectrum lies [21].

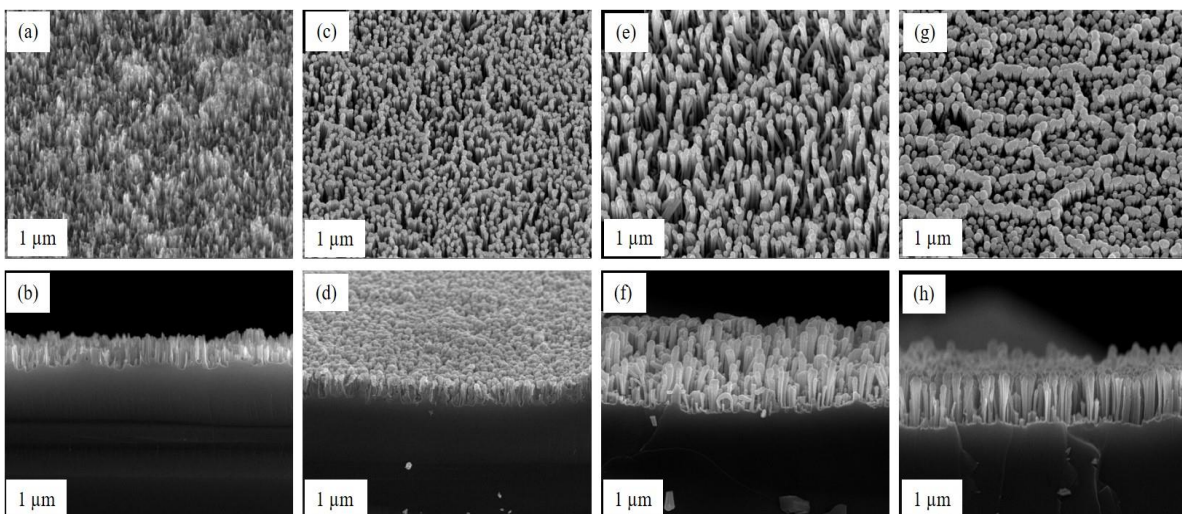
Figure 2 illustrates the top view and cross-sectional FESEM images for ITO films on planar c-Si reference samples. The figure indicates that the 50 nm ITO (Figure 2 (a) and (b)) possesses small grains. The grains are in the order of 10-15 nm in diameter. When the sputtered ITO thickness is increased to 80 nm (Figure 2 (c) and (d)), the grain size increases to about 20-25 nm. Some bigger grains are also visible, with around 50 nm in diameter. When the ITO thickness increases to 140 nm (Figure 2 (e) and (f)), a more uniform grain distribution can be observed. The grain size increases to around 60-65 nm. Other findings have also observed the increased grain size with a more uniform distribution in thicker ITO when sputtering ITO on the c-Si substrate [22,23]. Furthermore, columnar growth is also evident from the cross-sectional images.

Figure 3 illustrates the FESEM images (oblique and cross-sectional) of ITO film with different thicknesses deposited on b-Si. The oblique image shows that the b-Si nanowires fabricated by the MACE process are uniform and dense. The nanowires exhibit length of 500-570 nm and a width of 100-200 nm. When 50 nm of ITO is deposited on the b-Si nanowires (Figure 3 (c) and (d)), the nanowires are not fully covered by the ITO, and ITO appears like the surface capping of the nanowire tips. For the ITO with a thickness of 80 nm, the b-Si nanowires started to be covered by ITO (Figure 2 (e) and (f)) with improved conformality across the surface. The nanowires length increases slightly to about 1  $\mu\text{m}$  with a stiff base and wider top. No significant change in the width of the b-Si nanowires is observed. When the ITO film thickness is increased to 140 nm (Figure 3 (g) and (h)), the formation of self-conjoined hexagonal surface structures is observed (Figure 3 (g)). With this thickness, ITO completely covers the b-Si nanowires and the

regions between nanowires. This occurs when the length of the b-Si nanowires extends to about 1.1  $\mu\text{m}$ . This shows that more ITO is deposited on the b-Si nanowires than on the sides.



**Figure 2:** Top view and cross-section of (a and b) 50 nm ITO on p-type c-Si, (c and d) 80 nm ITO on p-type c-Si, (e and f) 140 nm ITO on p-type c-Si



**Figure 3:** Oblique ( $30^\circ$ ) and cross-section of (a and b) b-Si nanowires (c and d) 50 nm ITO on b-Si nanowires (e and f) 80 nm ITO on b-Si nanowires (g and h) 140 nm ITO on b-Si nanowires

To understand the elemental composition (weight percentages (wt. %)) of the sputtered ITO films (of In, O and Sn) on b-Si nanowires, EDX analysis is carried out. This is crucial to identify the composition of In, Sn and O on b-Si. It has been reported that Sn dopant concentration, together with an oxidation state of the  $\text{In}_2\text{O}_3\text{:Sn}$  matrix, controls the electrical parameters ( $R_s$ ,  $n_e$  and  $\mu_e$ ) of deposited ITO films for application in solar cells [23]. Figure 4 shows the EDX mapping of selected areas for b-Si nanowires (prior to ITO deposition) and ITO/b-Si nanowires with increased ITO thickness. The corresponding elemental mappings of the ITO/b-Si nanowires interface confirm the presence of In, O, and Sn elements with strong  $K_\alpha$  and  $L_\alpha$  peaks outlining the b-Si nanowires and are presented in Table 1. The EDX data shows wt.% intermixing between In, O, and Sn over the b-Si nanowires.

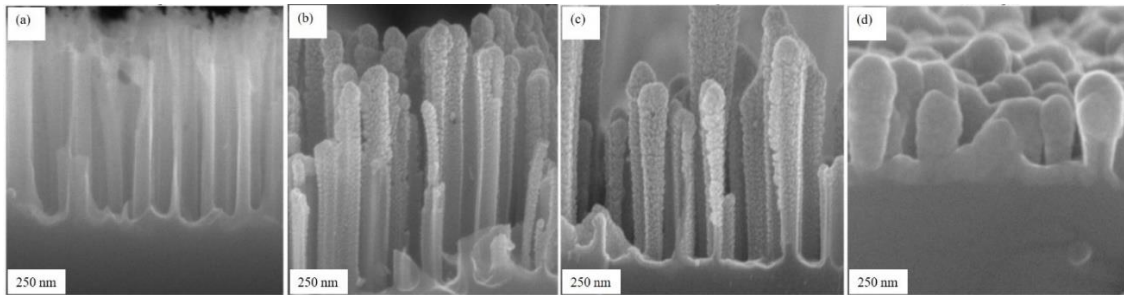


**Figure 4:** EDX elemental mapping of selected areas for b-Si nanowires and ITO/b-Si nanowires interface; (a) b-Si nanowires without ITO (b) b-Si nanowires with 50 nm of ITO (c) b-Si nanowires with 80 nm of ITO (d) b-Si nanowires with 140 nm of ITO

In Table 1, for 50 nm of ITO on b-Si nanowires, 37.41 wt.% of In and 16.68 wt.% oxygen with 0.4 wt.% Sn is observed on b-Si nanowires. Sample with 80 nm ITO thickness has 49.49 wt.% concentration of In and 22.32 wt.% oxygen with moderate Sn doping (3.1 wt.%). For a sample with 140 nm ITO, a nearly similar amount of In content (45.06 wt.%) is evident compared to the sample with 80 nm of ITO film. Although this sample has the lowest oxygen (9.14 wt.%) compared to other samples, it exhibits the highest Sn doping (4.22 wt.%). Therefore, the EDX results show that the samples with ITO films of 80 nm and 140 nm are characterised with Sn content in accordance with the uniformity criteria set for ITO films that can be used for application in ITO (n-type)/p-type c-Si heterojunctions as reported in the literature [14,24].

Characterisation of surface morphology of the reference b-Si nanowires (prior to ITO deposition) and ITO/b-Si nanowires are carried out using AFM and shown in Figure 5. B-Si nanowires demonstrate root mean square (RMS) roughness of 39.1 nm. After sputtering different thicknesses of ITO on the b-Si, RMS roughness shows an increasing trend; 49.5 nm, 66.2 nm and 77.5 nm, respectively. This shows a good corroboration with the FESEM results presented earlier. The increased RMS roughness with thicker ITO on the b-Si is due to the increased ITO thickness and grain sizes of the ITO films. This has also been reported by other work [5].

**Table 1** EDX (wt.%) of sputtered ITO with different thicknesses on b-Si nanowires

Elements	50 nm	80 nm	140 nm
	wt. (%)	wt. (%)	wt. (%)
Si K $\alpha$	45.51	25.09	41.58
In L $\alpha$	37.41	49.49	45.06
Sn L $\alpha$	0.4	3.1	4.22
O K $\alpha$	16.68	22.32	9.14
<b>Total</b>	100	100	100

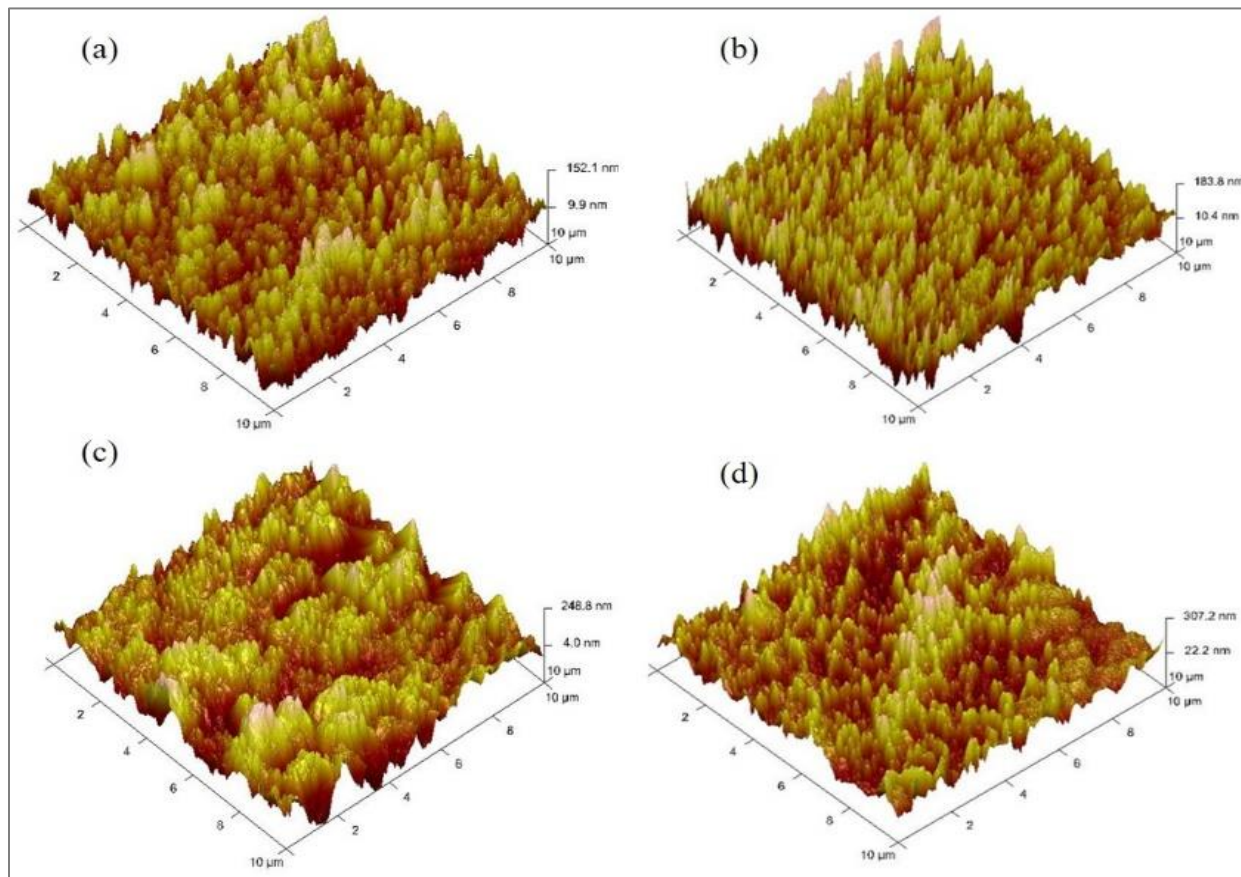


**Figure 5:** AFM images of b-Si nanowires (prior to ITO deposition) and ITO/b-Si nanowires with different ITO thicknesses; (a) b-Si nanowires (b) b-Si nanowires with 50 nm of ITO (c) b-Si nanowires with 80 nm of ITO (d) b-Si nanowires with 140 nm of ITO

Figure 6 (a) shows the total reflection and absorption curves of ITO films on planar c-Si for comparison to ITO on b-Si (Figure 6 (b)) within the 300-1100 nm wavelength region. For reference purposes, the total reflection and absorption curves of the planar c-Si (WAR of 40.0%) can be seen in our previous works [15,17]. Figure 6 (a) shows that all three ITO films on c-Si show low optical absorption and high surface reflection throughout the spectral region. ITO film of 50 nm shows nearly sinusoidal behaviour between 300-800 nm wavelength region. When the ITO film thickness is increased to 80 nm on p-type c-Si, absorption and surface reflection significantly improve with maximum values at around 450-650 nm wavelength region (close to the peak of AM1.5G solar spectrum). This is expected, as theoretically suggested by the principle of quarter-wavelength for ARC design ( $nd=\lambda/4$ ) [25]. When 140 nm of ITO is deposited on the c-Si, the sinusoidal behaviour of absorption and reflection is much more pronounced. Generally, WAR values of 22.1%, 17.2% and 19.5% are obtained for 50 nm, 80 nm, and 140 nm of ITO films on the c-Si.

In Figure 6 (b), the reference b-Si (prior to ITO deposition) demonstrates a WAR of 5.5% within the 300-1100 nm region with 94.5% optical absorption at a wavelength of 600 nm (not shown here) [15, 17]. After deposition of 50 nm, 80 nm, and 140 nm of ITO on the b-Si, the WAR decreases to 9.4%, 9.3% and 10.1%, respectively. The decrease in the WAR is attributed to the presence of light trapping in the b-Si, which enhances light absorption. When the incident light hits the b-Si nanowires after passing through ITO, the light passes through a homogenous medium with a refractive index ( $n$ ) that gradually increases between  $n$  of air ( $n=1$ ) to that of bulk c-Si ( $n=3.8$ ). Due to this, the reflection at the ITO/b-Si interface is suppressed, and light-coupling into the absorber is improved [26, 27]. From these results, it is also evident that there is an insignificant effect of different ITO thicknesses towards the reflection and absorption of the ITO on the b-Si.

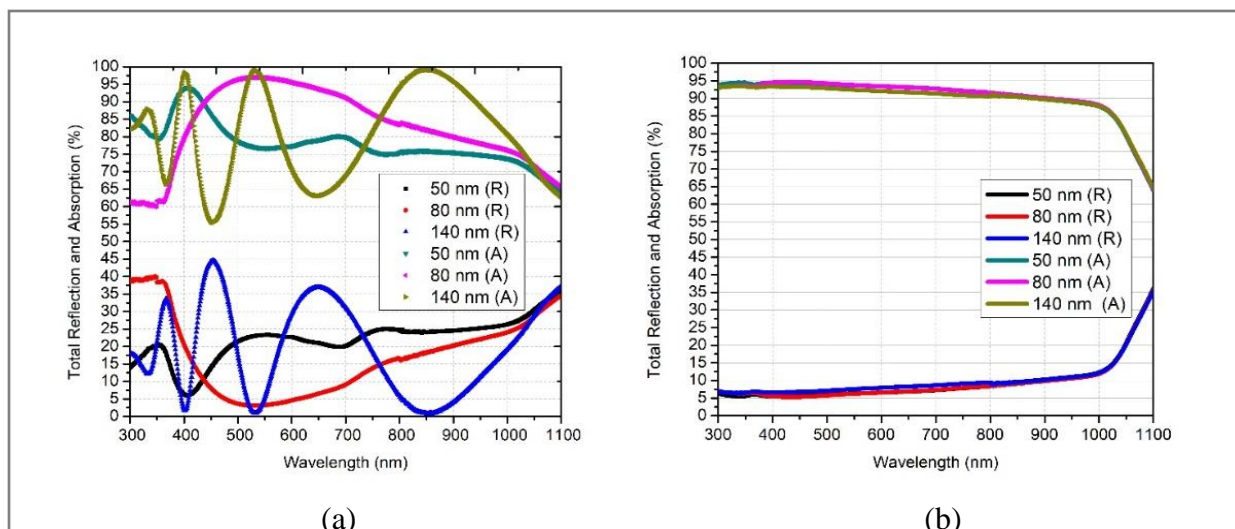


**Figure 6:** Reflection and absorption curves of 50 nm, 80 nm and 140 nm of ITO on; (a) c-Si reference (b) b-Si nanowires

Figure 7 shows carrier mobility ( $\mu_e$ ) and sheet resistance ( $R_s$ ) against carrier concentration ( $n_e$ ) of ITO with different film thicknesses on b-Si. The results represent an average of five points measurements on each sample. For samples with ITO film thickness of 50 nm,  $n_e$  of  $4.74 \times 10^{18} \text{ cm}^{-3}$ ,  $R_s$  of  $122.5 \text{ } \Omega/\text{sq}$ , and  $\mu_e$  of  $215 \text{ cm}^2/\text{Vs}$  are measured. For magnetron-sputtered ITO films, it has been reported that  $n_e$  increases with an increase in film thickness [22]. When the ITO's thickness on b-Si increases to 80 nm,  $n_e$  significantly increases to  $1.15 \times 10^{21} \text{ cm}^{-3}$ . This represents an  $R_s$  value of  $25.7 \text{ } \Omega/\text{sq}$ . However,  $\mu_e$  decreases to  $26.3 \text{ cm}^2/\text{Vs}$  due to the increased  $n_e$ . This could be attributed to increased charged impurity scattering as  $n_e$  is more than  $10^{20} \text{ cm}^{-3}$ , and grain boundary scattering as a change of ITO phase usually starts between 80-100 nm film thickness, even if the ITO is deposited at room temperature without subsequent annealing [28]. For the sample with 140 nm of ITO, although Sn dopant incorporation continues during deposition,  $R_s$  increases to  $118.1 \text{ } \Omega/\text{sq}$ . It is believed that this is contributed by the concurrent formation of the increased number of electrically non-active dopants ( $\text{Sn}^{2+}$ ) and their incorporation into the  $\text{In}_2\text{O}_3$  matrix on b-Si nanowires at an increased proportion. This causes a significant increase in  $\mu_e$  to  $208 \text{ cm}^2/\text{s}$  due to decreased  $n_e$  of  $1.7 \times 10^{19} \text{ cm}^{-3}$  ( $n_e < 10^{20} \text{ cm}^{-3}$ ), as also reported by other findings [20,21]. It is therefore established that when thicker ITO (80 nm and 140 nm) is deposited on b-Si, the  $R_s$  of the ITO increase due to low lateral conduction in the film. However, this can be viewed as an advantage as it causes a decrease in  $n_e$ , improving  $\mu_e$  for efficient heterojunction solar cells. The possible reason for the observed increase in  $R_s$  for 140 nm compared to 80 nm ITO on b-Si may rely on a simple physical model which suggests a complete change of state from amorphous to polycrystalline for ITO film thickness exceeding 100 nm as mentioned earlier [22]. When this happens, the structural defects on the surface of grains in the polycrystalline ITO layer yield charge carrier traps, which then reduce  $n_e$ .

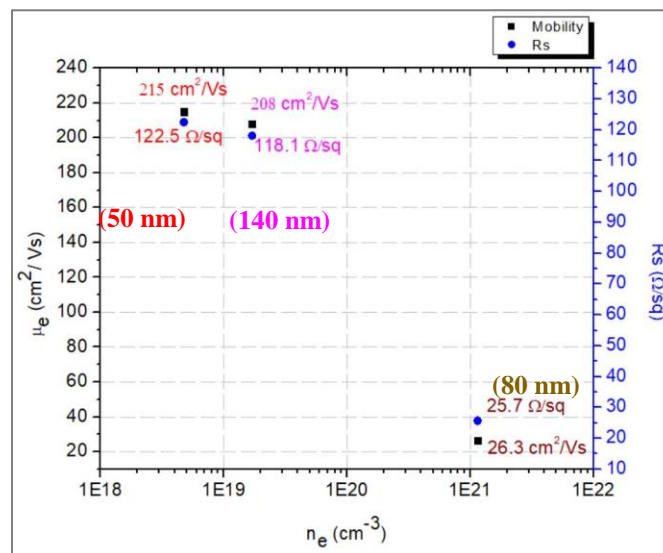


**Figure 7:** Carrier mobility (primary y-axis) and sheet resistance (secondary y-axis) with increasing carrier concentration (x-axis) for ITO with different thicknesses (50 nm, 80 nm and 140 nm) on b-Si

In summary, the sample with 50 nm ITO film on b-Si has optimum  $\mu_e$  but lowest  $n_e$  and highest  $R_s$ , while the sample with 80 nm ITO film possesses the highest  $n_e$  with the lowest  $R_s$  and  $\mu_e$ . A better trade-off between these parameters is seen for the sample with 140 nm of ITO on the b-Si. Therefore, Hall effect results reveal a trade-off between  $R_s$ ,  $n_e$  and  $\mu_e$  is necessary when deciding on ITO film thickness to be deposited on b-Si nanowires for potential application in ITO/c-Si-based heterojunction solar cells. Furthermore, from EDX analysis, ITO film of 140 nm is characterised by a similar In concentration observed for the 80 nm film thickness. However, the sample with 80 nm of ITO on b-Si demonstrates a lower concentration of Sn dopant atoms (3.1%) than the sample with 140 nm of ITO on b-Si nanowires (4.2%). As a result, 140 nm of ITO is chosen to fabricate ITO/c-Si/NiO (reference) and ITO/b-Si/NiO heterojunction solar cells.

Figure 8 presents the current-voltage curves for ITO/c-Si/NiO (reference) and ITO/b-Si/NiO solar cells. Under the white light illumination,  $J_{sc}$  of  $3.10 \mu\text{A}/\text{cm}^2$  and a corresponding  $V_{oc}$  value of 601 mV are demonstrated for the reference solar cell. Comparatively,  $J_{sc}$  of  $3.96 \mu\text{A}/\text{cm}^2$  and a corresponding  $V_{oc}$  value of 606 mV are realised in the ITO/b-Si/NiO cell. From the findings,  $J_{sc}$  enhancement of  $0.86 \mu\text{A}/\text{cm}^2$  (or 28% enhancement) achieved for ITO/b-Si/NiO solar cell is attributed to the enhanced light absorption due to the suppressed broadband reflection realised by the b-Si nanowires. This is supported by the WAR of 10.1% demonstrated by the ITO/b-Si interface compared to the WAR of 19.5% seen in the ITO/c-Si interface. In this work, the current-voltage behaviour shows a relatively low PV response from the solar cells due to white light illumination with low optical power ( $47 \text{ mW}/\text{cm}^2$ ) during the electrical characterisation.

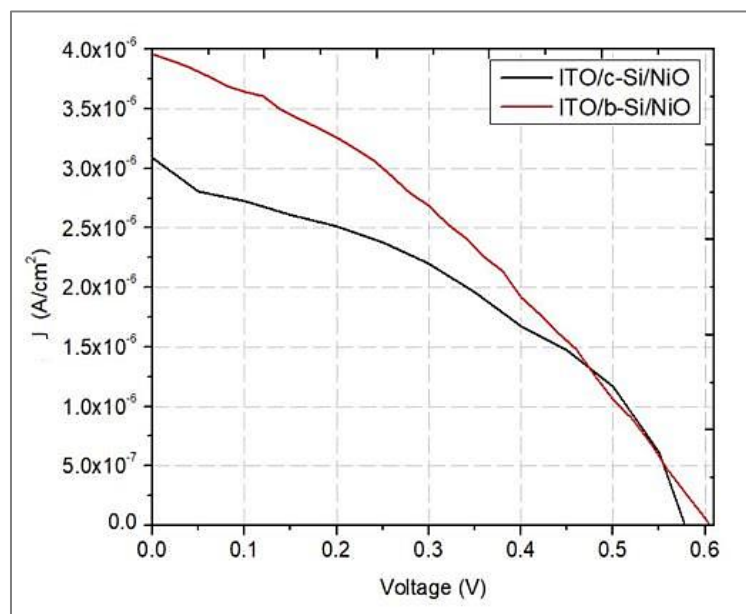


**Figure 8:** Current-voltage characteristics ITO/c-Si and ITO/b-Si solar cells measured under white light illumination (using LED-based solar simulator) at the illumination of  $47 \text{ mW}/\text{cm}^2$  and  $25^\circ\text{C}$

The relatively low PV response for both solar cells is anticipated since the LED-based solar simulator only produces its optical power within the 400-800 nm wavelength region [29]. Recently similar research findings have been reported in our previous work and by Kim et al. in related research [30, 31]. Kim et al. demonstrated that c-Si solar cells with an efficiency of 20% operated under standard testing conditions only demonstrate an efficiency of about 5% when operated under white light illumination (LED-based system). In this work, front Ag shading losses and parasitic absorption within the ITO in the short wavelength region (300-400 nm) could be another contributing factor to the low  $J_{sc}$  in the solar cells. Recently, Kim and Ozkartal et al. reported similar observations while investigating ITO/c-Si interfaces for applications in photodetectors and heterojunction solar cells, respectively [8, 32].

## CONCLUSION

This work investigates nano-optical properties of sputtered ITO on b-Si for heterojunction solar cells. The b-Si is fabricated using a two-step MACE process. The ITO films with a thickness of 50 nm, 80 nm and 140 nm have been sputtered on planar c-Si and b-Si. Besides, the ITO films have been deposited on a glass substrate. The ITO films' surface morphological and optical properties have been characterised using FESEM (with EDX analysis), AFM and UVVISNIR spectrophotometer within 300-1100 nm wavelength region. For 50 nm of ITO film on glass, a band gap of 4.0 eV is obtained, and the band gap is found to reduce to 3.90 eV and 3.85 eV when the thickness is increased to 80 nm and 140 nm, respectively. On planar c-Si, the FESEM image shows that 50 nm of ITO possesses small grains (about 10-15 nm). When the ITO thickness increases to 80 nm and 140 nm, the grain size increases to about 20-25 nm and 60-65 nm, respectively. At 140 nm, a more uniform grain distribution is evident. The FESEM image also illustrates that b-Si nanowires are uniform and dense, with a length of 500-570 nm and a width of 100-200 nm. For uniform ITO coverage on the b-Si, a thicker ITO is needed. However, thicker ITO results in increased nanowire length (about 1 $\mu$ m), a stiff base, and a wider top. For optical characterisation, the reference b-Si shows a WAR of 5.5% within the 300-1100 nm region. After deposition of 50 nm, 80 nm and 140 nm of ITO on planar c-Si, the WAR of 22.1%, 17.2% and 19.5% are obtained. When the ITO films are deposited on b-Si, the WAR decreases significantly to 9.4%, 9.3% and 10.1%, respectively, for the same ITO thickness. The lower WAR is due to the b-Si nanowires on the wafer surface. Hall effect results reveal moderate electrical parameters applicable for application in heterojunction solar cells for the sample with a thickness of 140 nm, with  $R_s$  of 118.1  $\Omega$ /sq,  $n_e$  of  $1.7 \times 10^{19} \text{ cm}^{-3}$  and  $\mu_e$  of 208  $\text{cm}^2/\text{Vs}$ . Under white light illumination (LED-based solar simulator), ITO/c-Si/NiO solar cell demonstrates  $J_{sc}$  of 3.10  $\mu\text{A}/\text{cm}^2$  and a corresponding  $V_{oc}$  of 601 mV. On the other hand, the ITO/b-Si/NiO solar cell exhibits  $J_{sc}$  of 3.96  $\mu\text{A}/\text{cm}^2$  and  $V_{oc}$  of 606 mV. The enhancement in  $J_{sc}$  of 28% achieved in the b-Si solar cell can be attributed to the enhanced light absorption within the 300-1100 nm wavelength region.

## ACKNOWLEDGMENTS

The authors want to acknowledge research funding through Short-Term Grant 304/PFIZIK/6315063 from Universiti Sains Malaysia (USM), Penang. The first author would like to acknowledge TetFund Nigeria and Umaru Musa Yar'adua University Katsina for PhD research scholarship.

## AUTHOR'S CONTRIBUTION

Auwal Abdulkadir conceptualised, and designed the research idea, performed data acquisition, and drafted and revised the current version of the submitted article to be published. Mohd Zamir Pakhuruddin supervised the research progress, revised the manuscript critically for important intellectual contents and approved the current version of the submitted article to be published. Azlan Abdul Aziz supervised the research progress and approved the current version of the submitted article to be published.

## CONFLICT OF INTEREST STATEMENT

The authors declare that they have no known competing financial interests or personal relationships that could have appeared to influence the work reported in this paper.

## REFERENCES

- [1] Kim, Hyunki, Lee, G. N., & Kim, J. (2018). Hybrid structures of ITO-nanowire-embedded ITO film for the enhanced Si photodetectors. *Journal of Nanomaterials*, 2018. <https://doi.org/10.1155/2018/4178989>
- [2] Park, W.-H., & Kim, J. (2016). Transparent and conductive multi-functional window layer for thin-emitter Si solar cells. *Materials Express*, 6(5), 451–455. <https://doi.org/10.1166/mex.2016.1331>
- [3] Ethar, Y. S., Asmiet R., Osama, A., Faizul, M. M. S., Nawal, M., Tarfa, A., Khalid, H. I. and Mohamed, H. E. (2022). In-depth optical analysis of Zn(Al)O mixed metal oxide film-based Zn/Al-layered double hydroxide for TCO application. *Crystals* 12(79), 1-10. <https://doi.org/10.3390/cryst12010079>
- [4] Aliyu, K. I., Ahmad, H. A., and Nayan, N. (2020). Structural optical and electrical properties of transparent conductive ITO / Al-Ag / ITO multilayer contact. *Beilstein Journal of*

- Nanotechnology*, 11, 695–702. <https://doi.org/10.3762/bxiv.2019.104.v1>
- [5] Zhucheng, J., Tiang, L., Xiaoyu, Z., and Jiaxiang, L. (2021). Optimization preparation of indium tin oxide nanoparticles via microemulsion method using orthogonal experiment. *Crystals* (11)1387, 1-13. <https://doi.org/10.3390/cryst11111387>
- [6] He, B., Wang, H., Li, Y., Ma, Z., Xu, J., Zhang, Q., Wang, D. (2013). Fabrication and characterisation of amorphous ITO/p-Si heterojunction solar cell. *Science China Technological Sciences*, 56(8), 1870–1876. <https://doi.org/10.1007/s11431-013-5287-1>
- [7] Simasshkevich, A., Dormidont, S., Leonid B., Nicolai C., Volker H., Marin R. (2016). Indium tin oxide thin films prepared by vapor phase pyrolysis for efficient silicon based solar cells. *Thin Solid Films*, 610, 35–41. <https://doi.org/https://doi.org/10.1016/j.tsf.2016.04.047>
- [8] Ozkartal, A. (2019). Characterisation of the ITO/p-Si/Al contacts produced by thermal evaporation. *Vacuum*, 168(July), 108799. <https://doi.org/10.1016/j.vacuum.2019.108799>
- [9] Von Gastrow, G., Ortega, P., Alcubilla, R., Husein, S., Nietzold, T., Bertoni, M., & Savin, H. (2017). Recombination processes in passivated boron-implanted black silicon emitters. *Journal of Applied Physics*, 121(18). <https://doi.org/10.1063/1.4983297>
- [10] Abdulkadir, A., Aziz, A. A., & Pakhuruddin, M. Z. (2019). Optimisation of etching time for broadband absorption enhancement in black silicon fabricated by one-step electroless silver-assisted wet chemical etching. *Optik - International Journal for Light and Electron Optics*, 187(May), 74–80. <https://doi.org/10.1016/j.ijleo.2019.05.019>
- [11] Noor, N. A. M., Mohamad, S. K., Hamil, S. S., Devarajan, M., & Pakhuruddin, M. Z. (2019). Effects of etching time towards broadband absorption enhancement in black silicon fabricated by silver-assisted chemical etching. *Optik - International Journal for Light and Electron Optics*, 176(July 2018), 586–592. <https://doi.org/10.1016/j.ijleo.2018.09.096>
- [12] Zhou, Z. Q., Hu, F., Zhou, W. J., Chen, H. Y., Ma, L., Zhang, C., & Lu, M. (2017). An investigation on a crystalline-silicon solar cell with black silicon layer at the rear. *Nanoscale Research Letters*, 12. <https://doi.org/10.1186/s11671-017-2388-y>
- [13] Marikkannu, S., Kashif, M., Sethupathy, N., Vidhya, V. S., Piraman, S., Ayeshamariam, A., Jayachandran, M. (2014). Effect of substrate temperature on indium tin oxide (ITO) thin films deposited by jet nebuliser spray pyrolysis and solar cell application. *Materials Science in Semiconductor Processing*, 27(1), 562–568. <https://doi.org/10.1016/j.mssp.2014.07.036>
- [14] Schulz, U., Kaiser, N., & Kley, E. (2010). Nanostructured SIS solar cells, 7725, 1–8. <https://doi.org/10.1117/12.854694>
- [15] Abdulkadir, A., Aziz, A. A., & Pakhuruddin, M. Z. (2020). Impact of micro-texturisation on hybrid micro/nano-textured surface for enhanced broadband light absorption in crystalline silicon for application in photovoltaics. *Materials Science in Semiconductor Processing*, 105. <https://doi.org/10.1016/j.mssp.2019.104728>
- [16] Mehmood, H., Bektaş, G., Yıldız, İ., Tauqeer, T., Nasser, H., & Turan, R. (2019). Electrical, optical and surface characterisation of reactive RF magnetron sputtered molybdenum oxide films for solar cell applications. *Materials Science in Semiconductor Processing*, 101(January), 46–56. <https://doi.org/10.1016/j.mssp.2019.05.018>
- [17] Abdulkadir, A., Noor, N. A. M., Aziz, A. A., & Pakhuruddin, M. Z. (2020). Broadband anti-

- reflection in black silicon fabricated by two-step silver-assisted wet chemical etching for photovoltaics. In *Solid State Phenomena* (Vol. 301 SSP, pp. 167–174). Trans Tech Publications Ltd. <https://doi.org/10.4028/www.scientific.net/SSP.301.167>
- [18] Pakhuruddin, M. Z., Huang, J., Dore, J., & Varlamov, S. (2017). Enhanced light-trapping in laser-crystallised silicon thin-film solar cells on glass by optimised back surface reflectors. *Solar Energy*, *150*, 477–484. <https://doi.org/10.1016/j.solener.2017.04.069>
- [19] Aliyu, K. I., Ahmad, H. A., Sadik, G. A., Muliana, T., Amaliyana, N. R., Anis, S. B., Nafarizal, N. (2021). Preparation of Sn-doped In<sub>2</sub>O<sub>3</sub> multilayer films on n-type Si with optoelectronics properties improved by using thin Al-Cu metals interlayer films. *Materials Science in Semiconductor Processing*, *131*(August). <https://doi.org/10.1016/j.mssp.2021.105870>
- [20] Untila, G. G., Kost, T. N., & Chebotareva, A. B. (2018). Fluorine- and tin-doped indium oxide films grown by ultrasonic spray pyrolysis: Characterisation and application in bifacial silicon concentrator solar cells. *Solar Energy*, *159*(October 2017), 173–185. <https://doi.org/10.1016/j.solener.2017.10.068>
- [21] Das, D., & Karmakar, L. (2019). Further optimisation of ITO films at the melting point of Sn and configuration of Ohmic contact at the c-Si/ITO interface. *Applied Surface Science*, *481*(March), 16–24. <https://doi.org/10.1016/j.apsusc.2019.03.074>
- [22] Fernández, S., Braña, A. F., Grandal, J., González, J. P., García, F., & Gómez-Mancebo, M. B. (2018). ITO-based selective contacts for silicon solar devices. *Proceedings of the 2018 12th Spanish Conference on Electron Devices, CDE 2018*, 3–6. <https://doi.org/10.1109/CDE.2018.8596978>
- [23] Ahmed, N. M., Fayroz A. S., Abdulgafour H. I., Ahmed A., Suleiman A. M. A. (2019). The effect of post annealing temperature on grain size of indium-tin-oxide for optical and electrical properties improvement. *Results in Physics*, *13*(102159), 1–6. <https://doi.org/http://doi.org/10.1016/j.rinp.2019.102159>
- [24] Ramaiah Subba, K. (2000). Optical, structural and electrical properties of tin doped indium oxide thin films prepared by spray-pyrolysis technique. *Semiconductor Science and Technology*, *15*(7), 676–683. <https://doi.org/10.1088/0268-1242/15/7/305>
- [25] Young, J. L., Jeha, K. (2022). Improvement of Electrical Properties of Sn-Doped Indium Tin Oxide by In-Situ Annealing. *Applied Sciences and Convergence Technology*, *31*(6), 156-160. <https://doi.org/10.5757/ASCT.2022.31.6.156>
- [26] Abdulkadir, A., Abdul Aziz, A., & Pakhuruddin, M. Z. (2020). Properties of indium tin oxide on black silicon after post-deposition annealing for heterojunction solar cells. *Results in Physics*, *19*, 103405. <https://doi.org/10.1016/j.rinp.2020.103405>
- [27] He, X., Li, S., Ma, W., Ding, Z., Yu, J., Qin, B., Qiu, J. (2017). A simple and low-cost chemical etching method for controllable fabrication of large-scale kinked silicon nanowires. *Materials Letters*, *196*, 269–272. <https://doi.org/10.1016/j.matlet.2017.03.131>
- [28] Li, S., Ma, W., Chen, X., Xie, K., Li, Y., He, X., Lei, Y. (2016). Structure and antireflection properties of SiNWs arrays form mc-Si wafer through Ag-catalysed chemical etching. *Applied Surface Science*, *369*, 232–240. <https://doi.org/10.1016/j.apsusc.2016.02.028>
- [29] Khatri, I., Amar, J. (2020) Morphologies and optical properties of black silicon by room

- temperature Reactive Ion Etching, *Journal of Materials Research bulleting*, Pre-proof. doi:10.1016/j.materresbull.2020.110973.
- [30] Arai, R., Furukawa, S., Sato, N., & Yasuda, T. (2019). Organic energy-harvesting devices achieving power conversion efficiencies over 20% under ambient indoor lighting. *Journal of Materials Chemistry A*, 7(35), 20187–20192. <https://doi.org/10.1039/c9ta06694b>
- [31] Kim, G., Lim, J. W., Kim, J., Yun, S. J., & Park, M. A. (2020). Transparent thin-film silicon solar cells for indoor light harvesting with conversion efficiencies of 36% without photodegradation. *ACS Applied Materials & Interfaces*. <https://doi.org/10.1021/acsami.0c04517>
- [32] Kim, Hong-Sik, Kumar, M., & Kim, J. (2018). Improved broadband photoresponse in Schottky-Like junction using carrier selective NiO contact on p -Si . *Solar RRL*, 2(12), 1800138. <https://doi.org/10.1002/solr.201800138>